On the role of chemical reactions in initiating ultraviolet laser ablation in poly(methyl methacrylate)

Manish Prasad, Patrick F. Conforti, and Barbara J. Garrison[a)]
Department of Chemistry, 104 Chemistry Building, The Pennsylvania State University, University Park, Pennsylvania 16802

(Received 2 March 2007; accepted 11 April 2007; published online 31 May 2007)

The role of chemical reactions is investigated versus the thermal and mechanical processes occurring in a polymer substrate during irradiation by a laser pulse and subsequent ablation. Molecular dynamics simulations with an embedded Monte Carlo based reaction scheme were used to study ultraviolet ablation of poly(methyl methacrylate) at 157 nm. We discuss the onset of ablation, the mechanisms leading to ablation, and the role of stress relaxation of the polymer matrix during ablation. Laser induced heating and chemical decomposition of the polymer substrate are considered as ablation pathways. It is shown that heating the substrate can set off ablation via mechanical failure of the material only for very short laser pulses. For longer pulses, the mechanism of ejection is thermally driven limited by the critical number of bonds broken in the substrate. Alternatively, if the photon energy goes towards direct bond breaking, it initiates chemical reactions, polymer unzipping, and formation of gaseous products, leading to a nearly complete decomposition of the top layers of substrates. The ejection of small molecules has a hollowing out effect on the weakly connected substrates which can lead to lift-off of larger chunks. Excessive pressure buildup upon the creation of gaseous molecules does not lead to enhanced yield. The larger clusters are thermally ejected, and an entrainment of larger polymer fragments in gaseous molecules is not observed. © *2007 American Institute of Physics*. [DOI: 10.1063/1.2740340]

I. INTRODUCTION

Ultraviolet (UV) ablation of polymeric and organic materials is of technological interest with applications ranging from medical diagnostics and treatment to fabrication of materials based on nanotechnology.[1–5] In particular, the ablation of poly(methyl methacrylate) (PMMA) has been extensively studied because of its many uses, e.g., as a semiconductor photoresist, an electronic packaging material, and a fixer in orthopedic surgery. It is even used as a model material to understand corneal material removal during LASIK surgery.[6] These applications employ lasers over a wide range of process parameters, i.e., wavelengths, fluences, pulse widths, and repetition rates, each yielding a different material response.[4,7–17] A unique feature of interest in far UV ablation of PMMA is the significant reduction in damage induced in the surrounding material following the ablation.[7]

Although a large database of experimental observations exists with regard to the ablation of PMMA, a definite agreement over how ablation proceeds is still elusive. A number of mechanisms have been proposed to interpret experimental results. Most of these can be divided into two broad classes: photothermal and photochemical.[7,18,19] In the case of a "pure" photothermal process, the photon energy is absorbed at specific sites (chromophores) along the polymeric chains. This energy is subsequently converted into heat, which may produce high temperatures and high mechanical stresses in the absorbing region, leading to thermal degradation of the material and causing massive ejection of the material or ablation.[20,21] Alternatively, in the "pure" photochemical excitation scenario, the photon energy is utilized to directly break bonds (photolytic scission) at absorption sites. This photofragmentation creates radicals and new molecular entities by chemical reactions, chemical degradation, high temperature and pressure and, possibly, ablation.[7,12,16]

The nature of photothermal and photochemical ablation themselves are subject to intense theoretical and experimental investigation. In the earliest models, Jellinek and Srinivasan proposed a Beer's law based dependence of the ablated yield on fluence,[22] following a complete photolysis of polymer chains. Later, they incorporated key processing parameters, such as pulse width and repetition rates, by proposing that a certain threshold level of absorbed photon concentration (ρ_T) is required in the substrate to take it to an electronically excited state and cause photofragmentation.[23] Below this threshold, the chromophores relax back to their ground state generating heat, which is effective only for short pulses. Above ρ_T, the photoproducts are formed and lead to ablation. Both of these models lacked microscopic insight into the ablation process. Atomistic scale studies[24] suggested that stress buildup and volume expansion in the substrate, caused by the formation of smaller molecules, play a key role in the subsequent supersonic ejection of the material. These small molecules have been observed in experiments using mass spectrometric techniques. However, the exact chemical composition of these small molecules in the ablation plume is still subject to much debate. In an earlier work, Srinivasan *et al.*[7] reported the predominant species to be MMA monomers resulting from polymer unzipping along with C_2 gaseous dimers, whereas others have reported CO,

a)Author to whom correspondence should be addressed; electronic mail: bjg@psu.edu

CO_2, CH_4, and CH_3OH as well as methyl formate.[13,15,25–28] This discrepancy has been attributed to the limited/selective sampling of the ablation plume as well as the availability of many possible photoexcitation pathways to the polymer chromophores at different photon wavelengths under different experimental conditions. This difference is discussed in more detail in the following sections. More recent photochemical models incorporate the change in the characteristics of the substrate[18,29] due to multiple photochemical modification pathways. At the other extreme, the thermal ablation models are built upon thermally activated bond breaking, creation of small molecules in the bulk, and surface desorption. These processes cause reduction in the cohesive energy of the polymer and removal of the material when the number of broken bonds exceeds a critical value.[18,20,30]

Real ablation process dynamics are rather complex, with both photothermal and photochemical pathways contributing to varying extents. Models incorporating both pathways have also been built.[19,31] However, even a coupled model with both these pathways lacks a comprehensive physical representation of the real process. In addition to these two pathways there are many other processes that can also occur simultaneously during laser irradiation. For example, mechanical stresses generated by high temperatures and creation of volatile species can cause ablation via mechanical failure[32–35] or, at the very least, alter reaction and activation energies governing thermal and chemical processes.[18,36,37] Other effects, such as variation of physical properties of polymer substrates with changing composition and screening of laser radiation by ablating plume, are also not straightforward to be described accurately in an ablation model. Given all these complexities, the primary aim of this work is to provide a qualitative microscopic insight into different physical pathways that can lead to ablation. Molecular dynamics (MD) is useful for providing us with this insight because it only requires a basic set of rules governing the material behavior, such as potentials which suitably describe the forces binding the polymer and energies involved in reactions,[38–40] as input. Moreover, MD has been used successfully to model thermal and photochemical ablation processes of molecular solids.[38,40–43]

Here, we focus our attention on the different processes occurring in the substrate and establish how they are responsible for the onset of ablation. We report MD simulations wherein laser energy is channeled into separate thermal and chemical excitation pathways to isolate the effects of the pure thermal process, i.e., just heating the polymer sample versus rapid photochemical decomposition of the substrate. The generation of mechanical stresses and other variations in the physical characteristics of the substrate that arise out of laser irradiation are an intrinsic part of the MD model, and their role in ablation is also analyzed. The reaction energies and kinetic rate expressions are included as part of a Monte Carlo (MC) reaction scheme to track the relevant chemical reaction kinetics occurring in the PMMA substrate. The aim is not to predict possible reactions following photoscission, but to incorporate a physically realistic description of chemical processes so that their impact on the substrate can be studied. In the next section we will give an overview of the MD-MC setup included in our model. It is followed by simulation results and a discussion about how ablation is initiated along different pathways.

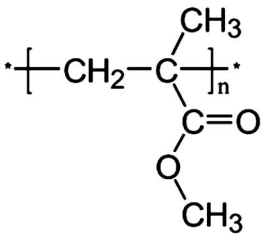

FIG. 1. The monomeric unit of the PMMA polymer is shown here. Each atom or group of atoms represents a coarse-grained bead in the simulation. Norrish type I correspond to a break in the CH_2–C bond, whereas Norrish type II is a break in the C–CO bond.

II. SIMULATION DETAILS

A. Polymer dynamics model

The MD simulation technique was used to study the initial stages of ablation in a PMMA matrix. Each polymer chain was made up of a set of coarse-grained "beads" or superatoms each representing a functional group.[43] This coarse graining permits the use of larger system sizes and longer simulation time scales compared to purely atomic systems. For PMMA, these functional groups are $CH_x(0 \leqslant x \leqslant 3)$, CO, and O, as shown in Fig. 1. Additional groups related to radicals and products formed (e.g., HCO, CH_4, and OH) are also part of the set of species. The bonding potentials between any two functional groups are of the harmonic form near the equilibrium bond lengths and are taken from Ref. 44. However, our simulations are expected to reach states far from equilibrium with high temperatures and pressures. All this can lead to bond breaks under realistic conditions. To accommodate these "thermally or stress induced" bond breaks, all bonding potentials (except those for double bonds) are switched to Morse potentials for bond lengths greater than 3% of equilibrium bond length.[43] Morse potential parameters are fitted individually to each bonding potential to ensure continuity in potential energy and forces. The angular potentials are of pure harmonic form and are also taken from Ref. 44. To prevent a sudden transition from finite angular potential to zero potential due to bond breaks, a screening function of the form $\exp(-2(r-r_0)^2)$ is employed for each of the two bonds forming a bond angle, where r is the instantaneous bond length and r_0 its equilibrium value. These screening functions are multiplied to angular potential energy functions, so that they go smoothly to zero as any of the two bonds are broken. The nonbonding inter- and intramolecular interactions are described using another Morse potential fitted to match PMMA physical properties, such as cohesive energy of the polymer.[43]

The starting sample is an amorphous polymer substrate made up of 951 PMMA chains, each of 19 monomeric units. The sample was prepared by starting with a low density polymer built by random insertion, followed by gradual compression to the bulk density according to the method described in Refs. 45 and 46. Each ablation simulation was

started with an initial temperature of 300 K and at the density of 1.2 gm/cm^3 ($51\times51\times936$ Å^3). Periodic boundary conditions were applied on the sides and a pressure absorbing boundary condition was applied at the bottom of the sample to prevent the downward traveling pressure wave from reflecting back into the sample.[47] These boundary conditions together mimic a deep substrate (i.e., no reflected pressure wave is formed at the back end of the sample at all times) at the center of the laser pulse where the mass and energy transfers are expected only along the depth of the sample. The detailed simulation methodology will be described elsewhere.[48]

B. Laser polymer interaction model

The laser pulse of wavelength (λ) pulse width (τ), and penetration depth ($1/\alpha$) was applied to the sample from $t=0$ to $t=\tau$. The photons are absorbed by the chromophores (–C– or –CO– in this case) in accordance with Beer's law. In order to isolate different mechanisms, the photon energy is directed into only one path in a simulation. This leads to one case where all the energy goes into heating the polymer; i.e., the photon energy is distributed over a monomeric unit (six beads as shown in Fig. 1) corresponding to absorption as kinetic energy. The other two cases are photochemical where photon energy is utilized to "directly" break two types of bonds. In the first case, the Norrish type I reaction (see Fig. 1), the C–CO bond on a PMMA side chain is broken. In the second case, the Norrish type II reaction, the C$-$CH$_2$ bond on a polymer's main chain is broken. The equilibrium bond strength in each case is 3.6 eV, so excess photon energy goes into kinetic energy of the beads involved in the bond cleavage. Upon a direct bond break, species with a broken bond are tagged as radicals and tracked for subsequent reactions. In addition to direct bond breaks, heating or stress induced bond breaks are also possible, as mentioned above for all cases. Following these thermomechanical bond breaks, however, the coarse-grained beads are not labeled as radicals in the simulation scheme and no subsequent reaction occurs.

The formation of radicals in the substrate leads to chemical reactions which can play an important role in ablation as mentioned above. There are a vast number of possible reactions that can take place during ablation given the high temperatures, stresses, and types of radicals. The selection of chemical reactions to form the basis set in our MC scheme is therefore crucial to the development of a feasible and realistic MD simulation scheme. The inclusion of too many reactions can easily slow down our MD time integration without adding any significant new physics to the ablation process. Our choice of a representative set of chemical reactions is based on the ablation products experimentally observed and the likely chemical reactions suggested in the literature.[7,8,10,11,13,16,25–28] As described in the introduction, the existence of small gaseous molecules such as CO, CO$_2$, CH$_4$, HCOOCH$_3$, and CH$_3$OH as well as MMA monomers and smaller polymer fragments in the ablation plume has been reported experimentally. The differences in observed products may arise from different starting radicals formed under different experimental conditions and following different reaction paths. At the base of the issue in these publications is whether PMMA is photolyzed at the main chain C$-$CH$_2$ bonding site (Norrish type II) or at the side chain C$-$CO/CO$-$O/O$-$CH$_3$ bonding site (Norrish type I), which determines what reactions take place after bond break and what products are formed. In order to understand the differences between the two Norrish-type bond breaks, their reactions, and the subsequent ablation, both these pathways have been simulated independently.

C. Chemical reaction model

The Norrish type I break (C–CO) proposed by Stuke *et al.*[15] is included in the set of reactions used in the present study. This break and the subsequent reactions give us the relevant ablation products likely from any side chain scission. All the reactions included can be categorized into six major types and are listed in Fig. 2. They are (a) hydrogen abstractions which can be performed by every radical depending on the availability of a hydrogen rich species nearby, (b) decarboxylation, (c) carbon monoxide elimination, (d) polymer unzipping into smaller fragments and monomeric MMA units, (e) CH$_3$ elimination followed by the formation of a double bond, and (f) a double bond formation for any two adjacent carbon radicals already joined by a single bond. Our aim in incorporating these reactions is not to try to predict what reaction will occur at high temperatures and stresses encountered in the polymer matrix, but to see how these reactions impact the polymer substrate and the ablation process. Electronic structure calculations were performed[49] to measure the activation and reaction energy for each of these reactions [except for (f) and second reaction in (a)]. The radical-radical recombination reaction listed in (f) above occurs without any activation energy barrier and reaction energy equal to the difference between strengths of a double bond and a single bond. The CH$_3$OH reaction energies were taken from *ab initio* calculations reported in Ref. 50. These reactions energies, computed based on first principles, will be used as an input to provide a physically accurate description of the chemical processes in the substrate.

As discussed above, the choice of the appropriate set of chemical reactions to add to our model is vital. In our earlier work,[51] the radical termination reactions via the formation of double bonds [reactions (e) and (f)] were excluded. This led to an almost indefinite continuation of hydrogen abstraction and unzipping reactions, extending to 1 ns, the total MD simulation time. The incorporation of radical-radical termination reactions significantly alters the ablation dynamics. It leads to rapid C=C formation, depletion of radicals from the system, and release of enormous amount of energy (2.76 eV per C=C bond formed). It also causes significant swelling, as opposed to little swelling observed previously.[51] The resulting swelling is also comparable to that in the pure heating case. In our current scheme, no polymer cross-linking reaction is included. This can be justified based (i) on the fast removal of the radicals from the substrate following reactions leading to short radical lifetimes, (ii) on the very small likelihood of cross-linking reactions occurring in the polymeric substrates over these short time scales due to

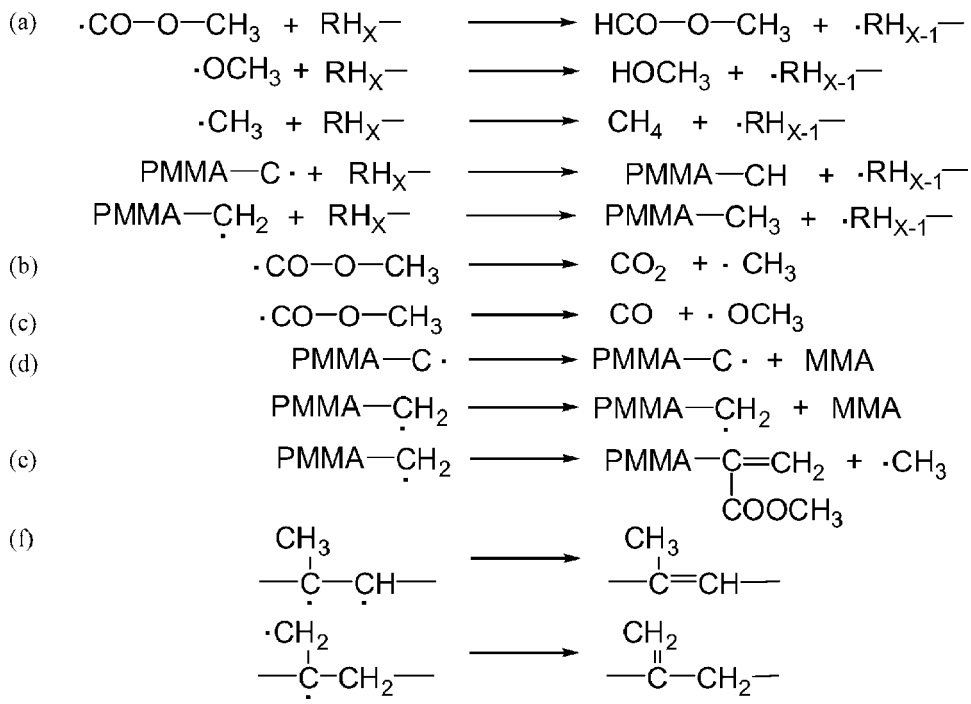

FIG. 2. Chemical reactions taking place in the substrate upon laser induced bond breaks.

steric hindrances, and partly (iii) on the lack of experimentally reported cross-linking reactions in PMMA.[10] Other possible radical-radical reactions involving smaller radicals (e.g., $^{*}CH_3$) are also not included as they lead to the formation of more varieties of small gas molecules, such as C_2H_6, without adding any new significant physics. The possibility of substrate modification leading to an incubation like effect[8,13,16,52] is also included in our photochemical scenarios—the carbon beads at a broken main chain site can form C=C, which can then absorb photons and convert it only to heat. For this effect, however, the laser pulse width would have to be long enough to allow for a sufficient number of double bonds to form. Note that not all the reactions occur in both Norrish-type bond break scenarios; e.g., reactions (b) and (c) occur only for Norrish type I bond breaks, whereas reactions (d) and (e) occur only for Norrish type II.

The reactions are carried out based on a MC scheme with predetermined Arrhenius reaction rates and formation energies. The reactions are performed during the MD simulation using a modified version of the coarse-grained chemical reaction model (CGCRM),[39,43] details of which will be described elsewhere.[48] Briefly, at every step, for every radical, all possible reacting species are identified within an interaction radius of 2 Å. If two radicals are next to each other, the corresponding radical-radical recombination reaction is selected and tried. Otherwise, the probability of the radical reacting is calculated based on its reaction rate (k_r) with each nearby reactant. Individual reaction rates k_r's are computed from the activation energy (E_A) of each reaction and local temperature (T_L) using an Arrhenius reaction rate expression:[43] $k_r = 10^{13} \exp(-E_A/k_B T_L)\ \mathrm{s}^{-1}$, where k_B is the Boltzmann constant. Next, one reaction pathway is selected for trial by drawing a random number. Finally, the selected reaction is tried; i.e., an assessment of the feasibility of the selected reaction is made by carrying out the reaction and measuring the corresponding energy difference. If this energy is within 10% of the desired chemical reaction energy, or 0.1 eV (depending on whichever is higher), the reaction is performed; otherwise, the species are reverted back to their original states and MD simulation continued. This measure introduces a physically realistic constraint when performing chemical reactions, ensuring that reactions only occur when conditions are suitable. Upon performing the reaction, the energy released (or required) is added to (or subtracted from) kinetic energies of the reacting species.

D. Simulation and analysis setup

All simulations were performed with $\lambda = 157$ nm laser (7.9 eV/photon) over a fluence range of 5–20 mJ/cm^2. Irradiation was carried out over a single pulse of varying pulse widths, $\tau = 5-150$ ps. The penetration depth $(1/\alpha)$ was set at 100 Å. The range of laser and material parameters selected here, i.e., for τ and $1/\alpha$ do not reflect real physical parameters. Experimental 157 nm lasers are currently available only in the power ranges suitable for longer nanosecond pulses,[53] while the effective penetration depth for PMMA interacting with 157 nm light is computed to be about 1200 Å.[54] The short 157 nm wavelength laser, short pulse width, and small penetration depth were chosen to maximize energy density in the substrate and the ablation yield along with any observable phenomena associated with the ablation process. The short wavelengths with higher energies are also known to enhance photochemical quantum efficiencies.[10] The choice of these simulation parameters may result in values that are not directly comparable to experiments for observable quantities such as the ablation yield and relative distribution of ablation products, as these quantities are

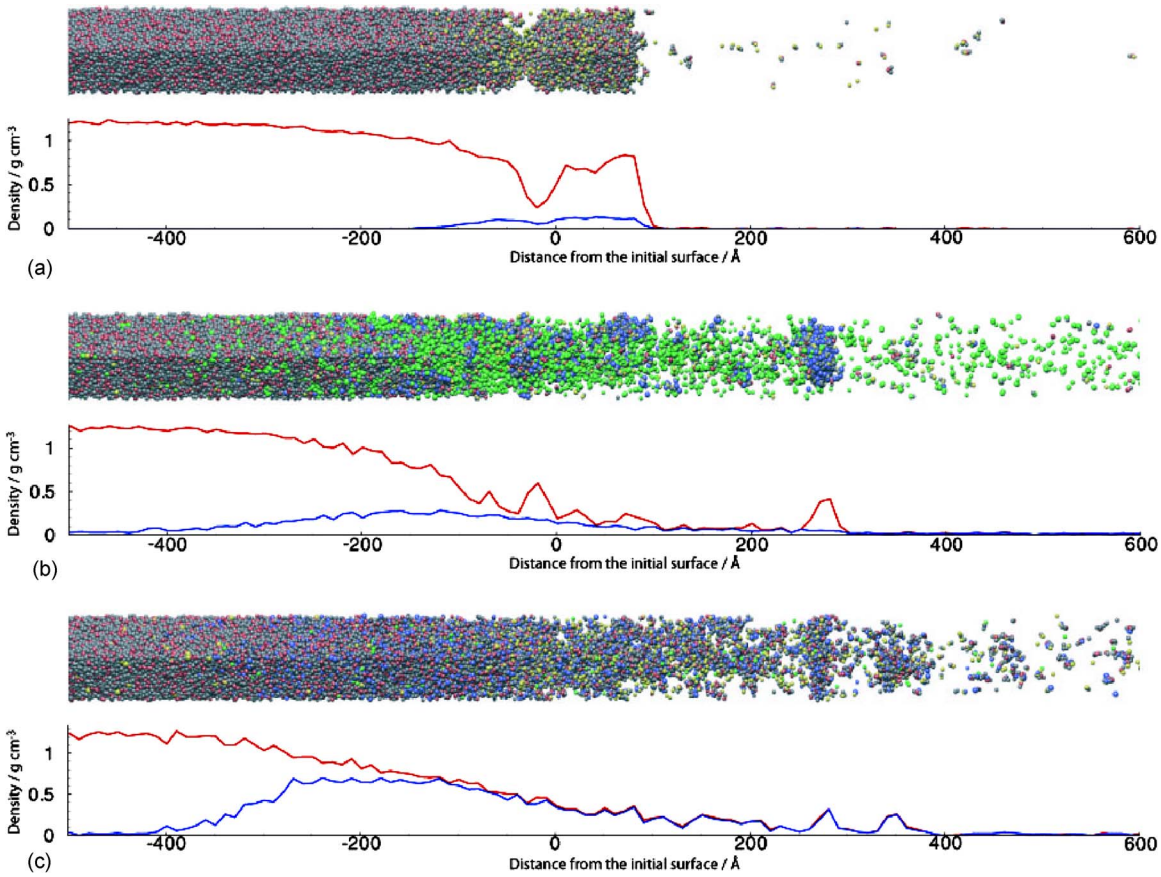

FIG. 3. (Color online) Snapshots from simulations for the three different cases: (a) heating (at 170 ps), (b) Norrish type I reactions (at 130 ps), and (c) Norrish type II reactions (at 150 ps). The fluence is 15 mJ/cm^2 and the pulse width is 150 ps. The gray circles correspond to coarse-grained beads in original polymer molecules, the yellow circles represent radicals and beads with thermally broken bonds, the green circles represent small gas molecules, and the blue circles represent double bonded carbon atoms. The associated xy plot shows full density (red) and contribution to density from thermally broken bonds, radicals, and gaseous particles, including monomer and polymer fragments (blue) as a function of distance from the initial surface.

highly dependent on the established energy density distribution. But, we expect the fundamental processes governing ablation, which are the subject of this article, to remain the same even though their relative importance may change with energy density distribution. In any case, a quantitative comparison of the ablation results is not the primary aim as, in each of the simulation reported here, the laser excites only a *chosen* portion of the ablation pathway.

The sample was dynamically sliced into slabs, each of 10 Å thickness, along the direction of the incident laser (z axis) for the purpose of evaluating properties of the substrate, such as density, temperature, pressure, chemical composition, and energy. The spatial density profile was used to further categorize the sample into two parts—bulk substrate and ejected plume—by identifying the dividing surface layer during the simulation. The exact value of the density used for this purpose is not critical to the identification and analysis of the substrate and the plume as the density drops rapidly at the interface during most of the ablation process. The yield was determined by counting all the particles in the plume. Two dimensional contour plots (t,z) of the material identified as bulk were prepared for a substrate analysis, with a time interval of 1 ps. The plume was also analyzed by dividing it into aggregates irrespective of their bead types or bonding state, based only on their spatial separation. For this purpose, an interbead distance of 5 Å was used to label interacting versus noninteracting beads as all the bonding potential energies go below the thermal energy available to a bead in the range of 3.5–5 Å. The clusters were identified by grouping together all the ejected coarse-grained beads found within a distance of 5 Å of each other. The average size is computed as the ratio of the second moment of cluster size distribution over its first moment. The simulations were followed over a period of 300–600 ps depending on the advancement of the ablation yield over time to ensure that we capture all possible large cluster ejection events.

III. RESULTS AND DISCUSSION

The existence of ablation was established first by taking snapshots of the MD simulation and computing yields of ejected beads. The snapshots of the early stages of ablation for all three energy deposition scenarios are shown in Fig. 3 for a pulse width of τ=150 ps and a fluence of 15 mJ/cm^2. The associated xy density plots in Fig. 3 are for the total mass density (red) and the mass density of "thermally" broken bonds, radicals, and all other newly created species as a result of reactions (blue). The snapshots indicate different evolution of the substrate, leading to ablation in each case. One large fragment is ejected in the heating case with very few small clusters. On the other hand, the substrate breaks

TABLE I. Ablation yields (and average sizes) expressed in number of equivalent MMA units ejected.

Fluence	Heat		Norrish type I		Norrish type II	
(mJ/cm^2)	5 ps	150 ps	5 ps	150 ps	5 ps	150 ps
8	23 (<1)	8 (<1)	1131 (198)	926 (147)	325 (1)	215 (1)
15	1258 (484)	1192 (769)	2260 (85)	2271 (136)	1461 (40)	1885 (26)
20	2145 (276)	2020 (511)	3275 (99)	3472 (63)	2079 (80)	2515 (72)

down into product gases (green circles) in the Norrish type I case, and into MMA units and smaller polymer fragments (blue circles representing C═C) in the Norrish type II case prior to ablation. Ablation in these two cases is initiated by ejection of these gas molecules and polymer fragments. The ejection time scales, 170 ps for the heating case, 130 ps for Norrish type I, and 150 ps for Norrish type II, also point to the different mechanisms at work. These differences in ablation profiles arise primarily due to the thermal and mechanical nature of the ejection process in the heating case, as opposed to the Norrish reaction cases, where the main process contributing to yield is cleavage of bonds, chemical reactions, and associated chemical disintegration of the polymer into new species. The presence of newly formed species, which make up a vital proportion of surface layers as seen in the xy plots in Fig. 3, plays a crucial role in initiating ablation, as we will discuss below.

The ablation threshold, located between 5 and 12 mJ/cm^2, emerges as the first common feature among all three scenarios. The calculated yields for each scenario as a function of fluence are reported in Table I. Ablation is established when irradiation results in the ejection of about 500–1000 MMA unit equivalents or 3000–6000 beads. A key characteristic of ablation, which sets this yield criterion of 500–1000 MMA units, is the ejection of large fragments of substrate comprised of hundreds of beads. This feature is fundamentally different from processes occurring below the threshold, where the ejected material is made up of smaller desorbed polymer fragments. No ablation is seen at the 5 mJ/cm^2 fluence for all cases (values not reported). At the fluence of 8 mJ/cm^2, small to negligible yields are observed for all, except for the Norrish type I case which ejected enough beads to attain ablation. There is variation in yield among the three energy deposition scenarios for a given pulse width and fluence, with heating cases consistently lowest and Norrish type I consistently highest. There is also a relatively large disparity in Norrish type II yields at any given fluence for 5 and 150 ps. Both of these differences can be explained based on the mechanistic aspects of the ablation process which are the focus of this paper. The values in Table I thus establish that yield is *not* a simple function of the pulse width for the short pulse widths studied.

The average size of ejected clusters given in parentheses in Table I coupled with simulation snapshots in Fig. 3 show that the largest clusters are ejected in the heating case along with very few small desorbed polymer fragments, e.g., less than 100 MMA units at 15 mJ/cm^2 fluence. The largest clusters, in the heating cases, also tend to stay together once they are ejected from the substrate due to lack of reactions in the plume. The clusters in the Norrish reaction cases are much greater in number, much smaller in average size, and dynamically evolving in nature; i.e., these clusters continue to break into smaller ones after ejection. For example, in the short pulse τ=5 ps, 15 mJ/cm^2 fluence, Norrish type I simulation, the average and maximum cluster size in the plume goes from 425 and 650 MMA units, respectively, at the time of ejection (20 ps) to 85 and 400 MMA units at the end of the simulation (400 ps). This evolution can be compared to the heating case where the average and maximum cluster sizes evolve from 683 and 867, respectively, at ejection times to 483 and 733, respectively, over the next 150 ps. This decrease, especially in average size, is due to the chemical composition of the ejected plume, with a large number of smaller gas molecules and polymer fragments present in the ejected surface layers, as seen the snapshots and density plots in Fig. 3. Also, the clusters in the Norrish type I case are bigger in size than the Norrish type II case because of the direct main chain $C-CH_2$ bond break in the latter. We now discuss the process and mechanism of ejection in each case.

A. Pure heating case

1. Ejection process

For the short τ=5 ps pulse width and fluences above 8 mJ/cm^2, the substrate experiences rapid heating, extreme pressure gradients followed by violent ablation of polymer matrix. These features can be observed in the contour plot in Fig. 4(a) which shows the evolution of pressure in the substrate as a function of depth and time for the fluence of 15 mJ/cm^2. The serrated profile of the top surfaces in these plots is due to the initial rise of the substrate and subsequent detachments of parts of the substrate as they become ablated. The first observable evidence of the ablation process is the significant surface swelling; e.g., Fig. 4(a) shows substrate swelling by about 170 Å, with the surface temperature reaching 4500 K within the first 10–30 ps, compared to less than 50 Å at 8 mJ/cm^2 where no ablation occurs. Figure 4(a) also shows buildup of a compressive pressure region at the laser penetration depth and generation of pressure waves which travel in both directions. The swelling is a direct consequence of the buildup of high temperature and compressive stress. A maximum pressure of 2.2 GPa is reached at the end of the 5 ps pulse, and a compressive pressure wave moves downward into the sample. This pressure wave is followed by a much weaker tensile wave formed as the compressive wave is reflected off the top surface. The tensile pressures attain values above the tensile strength of the material especially at these high temperatures.[35,55,56] These extreme thermomechanical conditions stretch the covalent bonds beyond their equilibrium values, forcing them to break. They also

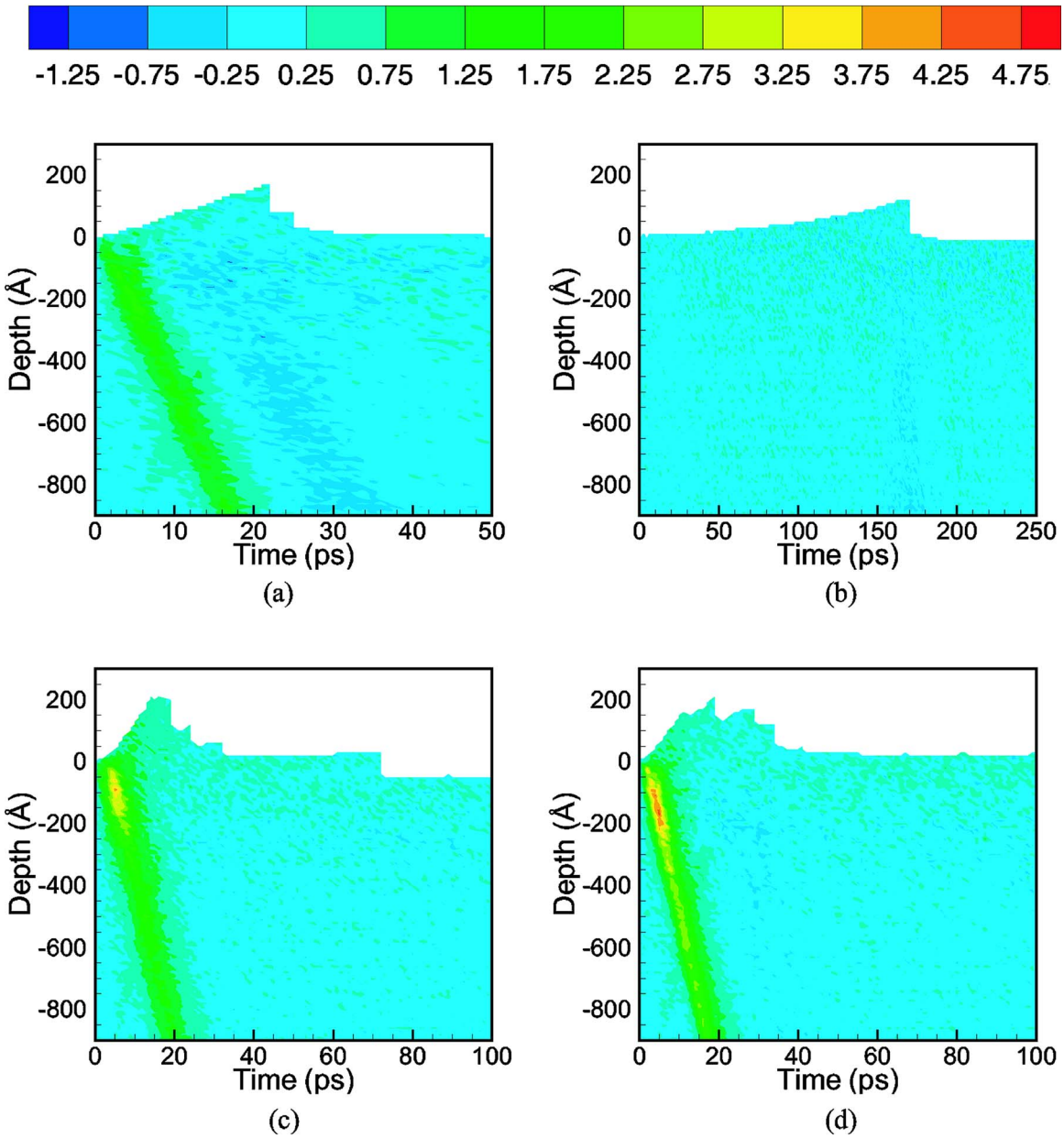

FIG. 4. (Color online) Contour plot of pressure (in gigapascal) as a function of depth from surface and time at the fluence of 15 mJ/cm^2 for (a) heating, τ=5 ps, (b) heating, τ=150 ps; (c) Norrish type I, τ=5 ps; and (d) Norrish type II, τ=5 ps.

weaken the long-range intermolecular interactions and reduce the cohesive energy of the substrate, thus fragmenting the substrate and leading to the generation of voids. The largest amount of substrate fragmentation is observed in the region located around the laser penetration depth, where the highest pressure values are attained. Ablation occurs at the end of this short time period when large hot chunks of material break off the surface as the density in top layers drops below 50% of the starting PMMA density. Once ejected, the rest of the substrate is substantially cooler with temperatures below 3000 K. The desorption process continues to eject smaller clusters over a period of 300–500 ps, further cooling the substrate to about 2300–2500 K. Thermal breakdown of the polymer matrix and evaporation are expected to continue over macroscopic time scales until the substrate is much cooler. Further discussion on the origin and significance of these high temperatures is given in Sec. III C.

The time scale of ejection for the 150 ps pulse is analogous; i.e., it also occurs within 10–20 ps of the end of the pulse, and the yields for both pulse widths are comparable as well. The ejection process, however, proceeds with a visibly different mechanism. The snapshot in Fig. 3(a) shows that until 170 ps only a few small polymer fragments are desorbed from the substrate, followed by ejection of a large chunk which makes up most of the ejected plume. More polymer fragments trapped underneath are released subsequently. The pressure contour plot in Fig. 4(b) shows a maximum pressure of only 1 GPa (for 15 mJ/cm^2 fluence). The maximum pressure reached is observed to be independent of laser fluences in the ablation regime. Also, no pressure gradients or high compressive pressure regions are formed and no pressure wave emanates. The maximum temperature in this case is 4500 K, which is the same as in the 5 ps pulse, but the swelling is much smaller at ~120 Å, as seen in Fig.

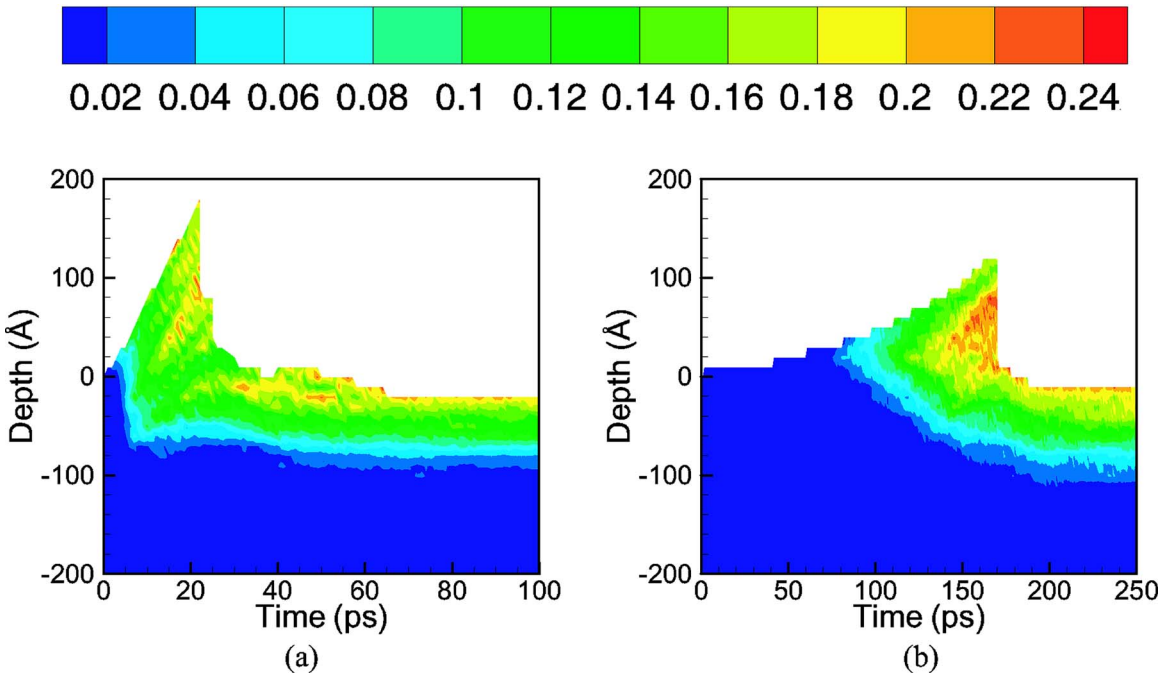

FIG. 5. (Color online) Contour plot of fraction of beads with thermally broken bonds per 10 Å layer as a function of depth from surface and time at the fluence of 15 mJ/cm^2 for (a) heating, τ=5 ps and (b) heating, τ=150 ps.

4(b). The swelling also proceeds more slowly in the absence of a strong compressive pressure buildup. The entire sample has an even distribution of the pressure close to a zero value for most of the simulation time scale, with the surface layers showing some negative values indicating tensile pressures due to lowering of the substrate density following swelling. These observations clearly rule out any direct role of mechanical stresses in driving the ejection process for the longer 150 ps pulse width.

2. Ejection mechanisms

The key reason for dissimilarity in the substrate evolution between 5 and 150 ps pulse widths is that the shorter pulse puts the system in a stress and thermally confined state, allowing extreme pressures and temperatures to develop within the polymer substrate.[32,35,40] The highest compressive pressure and temperature in the τ=5 ps case grows linearly with increasing fluence, causing faster surface expansion rates and larger swelling that eventually result in ablation via mechanical failure of the material. The effect of mechanical forces due to these high temperatures and pressures needs to be taken into account in building ablation models for these short laser pulses operating in stress confinement regimes. However, for the 150 ps pulse, the system is only thermally confined as there is little diffusion of thermal energy over the simulation time scale and the maximum temperature reached is the same as in the τ=5 ps case. No stress confinement is observed; thus, no high compressive pressure region is formed, ruling out the role of mechanical forces in ablation.

The mechanism of ejection for the longer pulse width was ascertained by examining the contour plots of the fraction of beads with thermally broken bonds per 10 Å layer as a function of depth and time for both τ=5 and 150 ps cases, as shown in Fig. 5. For the 150 ps pulse [Fig. 5(b)], the process of continuous thermal degradation of the polymer matrix is clearly seen in a gradual increase in this fraction starting after 100 ps of irradiation and reaching values of 0.25 before ejection. The density plot in Fig. 3(a) also shows the nearly homogeneous distribution of broken bonds in the top 200 Å of the swollen substrate just as the ablation starts. As seen in Figs. 5(a) and 5(b), these thermally activated bond breaks are present as deep as the laser penetration depth of the sample with a sharp boundary due to the exponential decay of laser energy deposition and temperatures attained with depth. They also indicate that for both pulse widths, the ejection of large polymer fragments corresponds directly to the attainment of a critical fraction of ~0.20 in the substrate; i.e., roughly one in every five beads has a broken bond. Further analysis reveals that up to 60%–75% of the broken bonds correspond to the main chain C–CH_2 bond cleavages which assist in the disentanglement of the polymer matrix, reducing cohesion and ensuing ablation. So, the mechanism of ejection is principally governed by thermally activated bond breaks in the case of the longer pulse width. In the τ=5 ps case, the critical fraction is less apparent as the high pressure gradient drives rapid void formation in the substrate, leading to material ejection.

The value of 0.2, for the critical fraction of beads with thermally broken bonds, corresponds to 0.10% or 10% of (covalent) bonds broken as every bond break leads to two beads with broken bonds. This value of critical bond break fraction is specific to the MD-polymer model used here, which has relatively short polymer chains (19 MMA units). Recent experimental studies[57,58] have shown that shorter chains have lower levels of entanglement, requiring fewer bonds to be broken for an efficient removal of monomers and polymer fragments by ejection. Longer chains with higher molecular weight will require a higher degree of decompo-

sition to achieve ablation. In addition, the PMMA chains are branched, where 2/3 of the bonds are present in the side chains (four per monomeric unit) and only 1/3 on the polymer backbone. The smaller share of main chain bonds, coupled with their preferential breakdown given above, points to a significantly larger fraction of main chain bond breaks (20%) compared to that of side chain bond breaks (5%). The polymer backbone is therefore four times as likely to break as the side chain, resulting in ablation at a relatively small *total* bond break fraction.

Further evidence of the role of the thermal ejection mechanism can be recognized in the common elements of the 5 and 150 ps pulse width simulations, such as similar yields and presence of the same critical number of bond breaks at the start of ablation. The ejection velocities and kinetic energies are much lower for $\tau=150$ ps even though they both eject similarly sized large substrate fragments. For instance, the largest cluster in each case at the 15 mJ/cm^2 fluence has velocities of 805 and 460 m/s and kinetic energies of 250 and 100 eV for the 5 and 150 ps pulses, respectively. Thus, the high pressure plays a key role in providing higher lift-off velocities and ensures a quick and efficient removal of the material. It implies that one can propose a model where the ablation process is primarily driven by thermal degradation of the polymer, and the role of pressure is confined only to driving away the ablated material.

The results of the simulations can be compared to models in the literature for thermal ablation. Bityurin and co-workers[18,20,21] have successfully used purely thermal models for polymer ablation in which the criteria for ablation is the attainment of the critical number density of broken bonds. Others have considered the critical energy density within the ablated volume.[12,59] Below, we will discuss each of these models and show that they can both describe the thermal ablation in our system.

In the bulk photothermal ablation model by Bityurin and co-workers,[18,20,21] the spatio-temporal evolution of the fraction of broken (covalent) bonds, n_b, is governed by[21]

$$\frac{dn_b}{dt} = V\frac{\partial n_b}{\partial z} + (1-n_b)k_0 \exp\left(-\frac{E_b}{k_B T}\right),$$

where k_0 is the preexponential factor, E_b is the energy required for breaking the bond, T is the temperature, and V is the velocity of the ablation front. The first term is for the removal of polymer fragments which have reached the critical fraction of broken bonds,[60] while the second term is for the generation of the fragmented substrate with broken bonds from the virgin polymer. The evolution of the total number of broken bonds before ablation sets in can be described using the above equation without the first term on the right hand side. For computational ease, we consider n_b to be the total number of broken bonds rather than the fraction, the difference being a factor of N, the total number of bonds. This evolution of the total number of broken bonds is shown in Fig. 6 for the 150 ps pulse width simulations at 15 and 20 mJ/cm^2 fluences. Also shown are the predicted values of n_b evaluated from least squares fits to parameters (k_0, E_b) based on the above equation. These fits were generated by minimizing the error in the time derivatives, with predicted

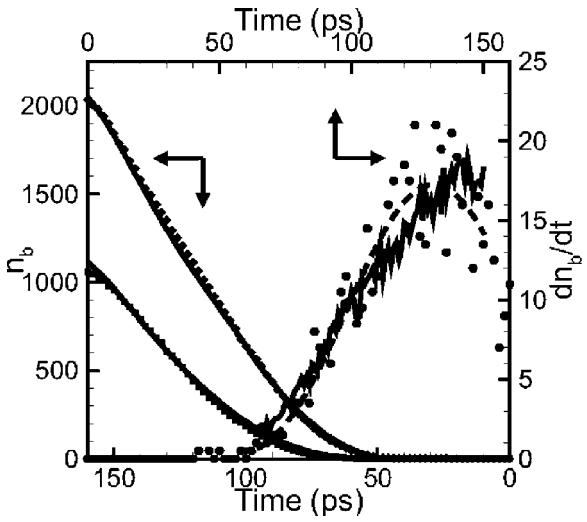

FIG. 6. The total number of broken bonds, n_b, vs time for fluences of 15 mJ/cm^2 (squares) and 20 mJ/cm^2 (diamonds) along with their least squares fits (solid lines). Also shown along the right and top axes are the derivatives dn_b/dt, for the 15 mJ/cm^2 fluence, computed from the numerical differentiation of raw data (circles), from the differentiation of polynomial fit to n_b (dashed line), and from the optimized fit to the polynomial's derivative (solid line).

dn_b/dt values based on the above equation summed over all spatial bins (along z) and actual dn_b/dt values computed from an analytical fit to the evolution of n_b with time. The spatiotemporal distribution of temperature used in integrating the above equation was taken directly from the simulation data instead of solving the heat transfer equation. Also, the evolution of the total number of broken bonds, n_b, was used instead of the complete profile of the number of broken bonds as a function of space-time (t,z) because the latter has significant variations in the derivative term dn_b/dt over the range of spatial bins at any given time point. The evolution of the former is smooth, as seen in Fig. 6, which is used to compute a polynomial fit and its analytical derivative.

A least squares fit over both the 15 and 20 mJ/cm^2 fluences yields the parameter set (2.02×10^{12} s^{-1}, 2.08 eV) for (k_0, E_b). Clearly, the fits to n_b and dn_b/dt, as shown in Fig. 6, capture their evolution well and provide a good description in terms of a thermally activated bond break process. The E_b values are lower than the C–C bond strength of 3.6 eV due to the softening of the covalent bonds at high temperatures; i.e., the thermal bond break process only acts on the polymeric substrate which is far from its equilibrium state, where the effective interaction energy is much lower due to the Morse potential based weakening of the covalent bond energies. This analysis is further supported by the fact that high temperatures are established rapidly throughout the ablation volume while the bond break process starts much later (see Fig. 6 for the time scale of the bond break process). The values of (k_0, E_b) obtained here are comparable to those published in Ref. 21, where the values of (3.57×10^{12} s^{-1}, 1.5 eV) were used as parameters in the bulk photothermal ablation model for polyimide. The description of the spatial (z) profile of the number of broken bonds also agrees well with the simulation data (not shown), even though it was not included explicitly in the fitting process. The spatial profile, taken at the end of

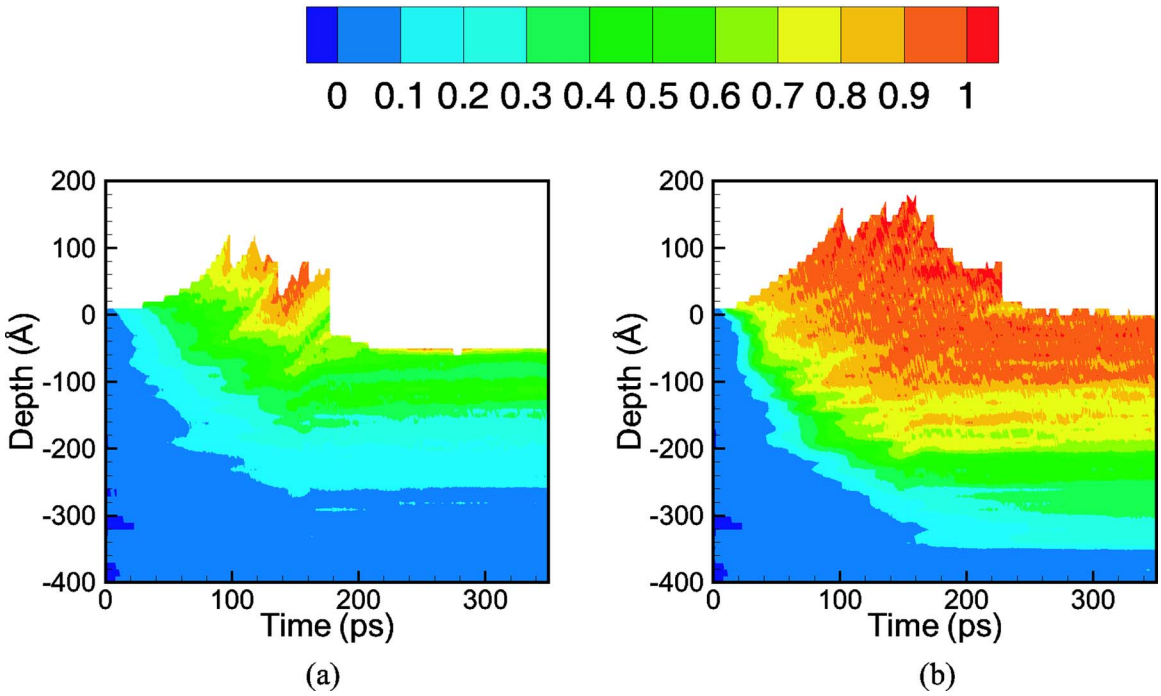

FIG. 7. (Color online) Contour plot of the fraction of beads representing the transformed substrate per 10 Å layer as a function of depth from surface and time at the fluence of 15 mJ/cm^2 and τ=150 ps for (a) Norrish type I and (b) Norrish type II.

the laser pulse, coupled with the critical bond break fraction of 0.10 as determined from the information in Fig. 5 indicates ablation depths of 59 and 110 Å compared to the actual ablated depths of 62 and 105 Å at 15 and 20 mJ/cm^2 fluences, respectively. The agreement is excellent, and it demonstrates that the thermal bond break model can be used as a tool to analyze the ablation process as well as predict the process dynamics.

Volumetric energy density established by the laser inside a polymer substrate can also be used as a guide to understand and predict ablation.[12,59] The interpretation of energy density for a polymer, however, is complex because there are strong covalent bonding interactions within the chains as well as weaker van der Waals interactions between the chains. In our earlier work, based on the same simulation setup,[61] it was shown that imparting 5 eV/monomer (8 mJ/cm^2) in the surface layer of one penetration depth only led to surface evaporation and insufficient void generation or fragmentation of the substrate and no ablation. At a higher fluence, with 5.9 eV/monomer (10 mJ/cm^2), ablation was initiated which corresponded to a critical energy density of 0.037 eV/Å^3. The role of this established energy density can be understood as follows. At the 15 mJ/cm^2 fluence, 1192 MMA equivalents are ejected, which correlates well with 1142 broken (covalent) bonds at the ejection time of 170 ps and 1564 at the end of the simulation at 427 ps. *Assuming* that all the ejected materials come from the region with a broken bond fraction greater than the critical value[18] and one main chain bond break occurs per MMA unit, we get 1192 bond breaks within the ablated region. This number corresponds to $1192 \times 3.6 = 4291$ eV of energy required for bond breaks within 62 Å of ablated depth. Given the area of the substrate illuminated by the laser, the energy required for bond breaks corresponds to an energy density of 0.027 eV/Å^3 in the ablated region. We arrive at the same energy density value for the 20 mJ/cm^2 fluence. This close agreement reflects the equivalence of two approaches, with the established energy density directly contributing to the thermal softening of polymeric bonds, the bond break process, and the kinetic energy of the ejected substrate. The comparison of energy densities presented here ignores the long-range intermolecular interactions which are inherent in the polymeric materials.[18] For example, it has been reported that the energy density required to achieve ablation is higher in the case of longer chain polymers.[57,58] Thus, the value of energy density computed based only on strong covalent bonds represents a firm lower bound on the critical energy density.

The analysis above illustrates how the thermal models considering broken bond density[18,20,21] and critical energy density[12,59] both provide coherent descriptions of the ablation volume for polymers. The MD simulations provide a self-consistent mechanism for observing the fundamental physics, proposing physical models and estimating values of the process parameters. The bulk photothermal model can be used to predict ablation characteristics once the predominantly thermal nature of the ablation process has been established.

B. Norrish reaction cases

1. Ejection process

For the Norrish-type bond breaks, the laser irradiation leads to the generation of radicals followed by a chemical transformation of the substrate, as shown in the contour plots in Fig. 7. The transformed substrate is composed of beads representing radicals, broken polymer fragments, and newly formed molecules. Their distribution was analyzed by dividing the substrate in 10 Å slices and measuring the fraction of

the transformed material (TF). A value of unity in each case corresponds to a complete decomposition of the original polymer matrix in that layer. In Fig. 7(a), for Norrish type I reactions, the green region ($0.4<\mathrm{TF}<0.6$) is formed, following photolysis and reactions given in Sec. II C. The maximum transformation does not approach unity because only the cleaved side chains are involved in subsequent reactions. The orange-red region ($\mathrm{TF}>0.8$) in the swelled part of the substrate corresponds to higher concentrations of small molecules ejecting outwards which can also be seen in Fig. 3(b). In Fig. 7(b), for Norrish type II reactions, the green region is formed in a similar fashion, following photolysis and initial reactions. The change to orange and then red occurs as the main chain radicals undergo unzipping, forming MMA monomers. Even a small fraction of main chain radicals can gradually lead to a complete transformation of the region due to the self-propagating nature of the unzipping reaction and the high temperature in the top layers.

A rapid and complete transformation of the upper layers occurs during the irradiation time scale. The resulting chemical damage penetrates deep in the sample, up to 250 and 350 Å under the original surface, as seen in Fig. 7, for Norrish type I and Norrish type II, respectively, at the 15 $\mathrm{mJ/cm^2}$ fluence and 150 ps pulse width, compared to just 100 Å for the corresponding heating case. It was found that most of this transformation occurs quickly within the first 10–20 ps after bond breaking and occurs even below the ablation threshold. For example, in the case of Norrish type II reactions, a steady distribution of about 200–250 double bonded carbons (C═) per 10 Å layer is observed in top 150–200 Å, corresponding to the complete transformation of those layers, at fluences just under the ablation threshold, but they do not eject directly. The snapshots and density profiles in Figs. 3(b) and 3(c) show the surface layers entirely composed of these newly formed species at the start of ablation. Figures 3(b), 3(c), 7(a), and 7(b) also show that in the case of Norrish reactions the onset of ablation occurs during the laser irradiation, whereas it is delayed until after the pulse is over in the case of heating. The onset is hastened due to the generation of small molecules which start streaming out of the substrate as soon as they are formed. For the shorter 5 ps pulses, the contour plots are not shown because reactions lead to an almost complete transformation of the substrate surface within 15 ps before the start of ablation as viewed in the surface profiles of Figs. 4(c) and 4(d). The postablation profile given in Fig. 7 shows leftover surface layers ~200 Å under a surface primarily composed of the newly formed species. The postablation profiles for 5 ps pulse Norrish reaction cases are similar to those of the longer 150 ps pulses.

There are differences in the nature of transformation of substrates between Norrish type I and II reactions. In the case of Norrish type I, the primary products are CO, CO_2, CH_4, CH_3OH, and $HCOOCH_3$. These volatile gas molecules start streaming out of the swollen polymer matrix immediately. The polymer chain remains largely intact with possible double bonds or –CH–groups at the side chain scission sites. The residual substrate is at a lower density (~0.7–1.0 $\mathrm{gm/cm^3}$) than the original bulk, in a disentangled state after the loss of most of the side chains, and with much reduced cohesive energy density. For Norrish type II reaction, on the other hand, the primary products of reactions are the MMA monomers and smaller polymer fragments with some CH_4. These are not able to escape as rapidly as the smaller, more volatile Norrish type I products and end up causing larger swelling of the polymeric substrate as witnessed in Fig. 7(b) versus 7(a). The resulting substrate is also of much lower density (~0.6–0.7 $\mathrm{gm/cm^3}$) and lower cohesive energy. Another difference, in the case of Norrish type II reactions, is the initiation of unzipping reactions which creates double bonded (C═C) MMA units and propagating radicals for additional unzipping of polymer chains extending the damage further and deeper into the sample. The presence of these sites leads to about 35% and 55% of the incoming photons (at 15 $\mathrm{mJ/cm^2}$ fluence) being absorbed by these double bonded carbon centers for the 5 and 150 ps pulse, respectively. Since no multiphoton absorption happens in our simulation scheme, this effect is not seen in the Norrish type I case. The photons thus absorbed can only generate heat, making the substrate with Norrish type II reactions hotter by about 300–400 K. Consequently, fewer direct bond scissions are registered for Norrish type II which affects the yield reported in Table I.

The chemical reactions release a large amount of heat—especially the exothermic double bond formation—which, along with the residual photon energy following Norrish-type bond breaks (about 4 eV/photon for 157 nm laser), is absorbed as heat in the substrate. This large energy input makes these scenarios far from being purely photochemical in nature. Future studies with longer wavelengths (e.g., 248 nm) are in progress to address this issue. For the 15 $\mathrm{mJ/cm^2}$ fluence, for $\tau=5$ and 150 ps, respectively, the highest temperatures reached in the Norrish type I substrates are 3800 and 4200 K vs 4200 and 4500 K for Norrish type II substrates. This large temperature range arises due to the redirection of part of the laser energy from bond scission to the thermal pathway mentioned above, the duration of the reactions which is directly related to pulse width and the differences in the reaction energies, and the rate of formation and removal of small molecules. Even after ablation is over in both Norrish reaction cases, the surface temperatures are high (2000–2800 K), just as in the heating case. So, the thermal breakdown, unzipping reaction, and evaporation of small molecules along with polymer fragments trapped just underneath the surface can continue over a much longer time scale.

The contour plot of pressure as a function of depth and time is shown in Figs. 4(c) and 4(d), at a fluence of 15 $\mathrm{mJ/cm^2}$ and a $\tau=5$ ps pulse, for Norrish type I and II cases, respectively. In both cases the pressure developed linearly increases with increasing fluence (stress confinement regime), reaching highest values of ~4–5 GPa, about twice the value seen in the heating case. The primary source of the greater pressure wave amplitude is the large number of small molecules, as the highest temperatures reached are similar to the heating case. This effect has been termed as the thermochemical pressure generation,[35] caused by a large number of small and volatile polymer breakdown products with larger

unit atomic volumes.[24] In Figs. 4(c) and 4(d), a compressive pressure wave can also be seen traveling down the substrate as well as contributing to the swelling of the top surface. At 15 mJ/cm^2 fluence, 100–200 Å swelling of the substrate can be seen in Figs. 4(c), 4(d), 7(a), and 7(b) and compared to little or no swelling observed below the threshold fluence, with less than 50 Å at 5 mJ/cm^2. The rapid chemical reactions and generation of small molecules also initiate the swelling process earlier and faster than in the heating case. However, in all Norrish reaction cases, little or no subsequent tensile wave emanates from the surface following the fast expansion, unlike the heating cases. This difference is attributed to an almost complete transformation of the top surface from an amorphous polymer matrix to a dense mixture of small gaseous molecules as described above. The gas phase at high surface temperatures and densities of $\sim$0.6 gm/cm^3 does not result in tensile pressure generation when the upward moving pressure wave reaches the top surface. No high pressure region or pressure waves were observed for the longer τ=150 ps pulse for any of Norrish reaction simulations, analogous to the pure heating case.

2. Ejection mechanisms

For the shorter pulse, the ejection process in Norrish reaction cases is primarily governed by high surface temperatures and compressive pressures driving violent ejection of gases and polymer fragments off the substrate. The larger fragments eject later followed by gases trapped deep inside the substrate. For the longer pulse these two different regimes are clearly visible. Once again, the first visible sign of impending ablation is a significant surface swelling. Then, hot gases, in the Norrish type I case, formed just underneath the top layers of the substrate stream out as soon as they are formed. The decomposition of the substrate and the lowering of the surface density resulting from swelling aid in the ejection process. These gas molecules eject with high velocities up to several km/s depending on the fluence. The gases present deeper in the sample attempt to diffuse out as well though with lower thermal energies. The loss of these gases hollows out the already disconnected substrate. Next, the larger polymer fragments eject with much lower velocities, followed by more trapped gases. In the Norrish type II case, the ejection occurs in a more layerwise manner with polymer fragments near the surface with high energies ejecting rapidly, followed by the ejection of slower moving, larger aggregates of polymer fragments.

While the small molecules are ejected primarily because of their volatile nature and high temperatures, the likely mechanism of ejection of larger chunks could be many—microscopic fluctuations in pressure, high thermal energies, and/or the upward momentum of the gases trapped deeper in the sample. As mentioned before for the heating case, the similarity in the total yield at both pulse widths rule out any significant role of the laser generated compressive pressure wave in the ejection of this material, except in providing higher ejection velocities. The ejection of the largest clusters is much delayed in Norrish reactions as opposed to heating case, further diminishing the role of this pressure in their lift-off. The upward momentum of the trapped gas is also ruled out as the motion of upper layers of gas molecules at high velocities appears decoupled from the much slower moving larger fragments. Moreover, the amount of gas trapped underneath the larger ejected chunks is small, as observed in the evolution of total yield following the ejection of big chunks. It is likely some large clusters ejected *earlier* in the ablation process do get accelerated or carried away by ejecting gas molecules. But the larger clusters ejected *later* definitely do not appear to be accelerated. Their ejection itself could then only be directed by a thermally activated process, i.e., high thermal energies giving rise to microscopic, localized, and transient pressure fluctuations resulting in a concerted upward motion of a large fragment of the hollowed out substrate. The likelihood of this mode of ejection is further supported by similar uplift velocities of the largest clusters which are in the range of 50–150 m/s for both reaction types and both pulse widths.

A two step ejection process similar to the one described here has been proposed earlier by Kalontarov and Marupov.[62] In their model, the photochemical ablation is described as a continuous surface process (i.e., a relatively small penetration depth) occurring during laser irradiation. The first step corresponds to the destruction of polymer macromolecules via photolysis, followed by the second step of removal of debris or photoproducts via a thermally activated process. Following the removal, the laser interacts with a fresh polymer substrate deeper in the sample, and the process continues. The variation of the concentration c of photoproducts (i.e., transformed material) in the reaction volume was given by[62]

$$\frac{dc}{dt} = \frac{I\varphi\varepsilon_0}{h\nu}(c_0 - c) - ck\exp\left(-\frac{E}{k_B T}\right),$$

where the first term is for the generation of transformed materials based on $h\nu$, the energy of a photon, I, the fluence, φ, the quantum yield, ε_0, the extinction coefficient, and c_0, the initial concentration, while the last term denotes a thermally activated removal with k, the rate constant, and E, the activation energy. Rewriting the above equation in terms of n, the total number of transformed beads, n_0, the initial number of beads, and n_p, the number of incident photons per picosecond, we obtain

$$\frac{dn}{dt} = k_\varphi n_p(n_0 - n) - nk\exp\left(-\frac{E}{k_B T}\right),$$

where k_φ is the rate constant for the photochemical transformation process. The evolution of the total number of transformed beads, n, along with the least squares fits based on the above equation with respect to parameters (k_φ, k, E), is shown in Fig. 8 for both Norrish reaction cases at 15 mJ/cm^2 fluence and τ=150 ps pulse. The fits were generated by minimizing the error between the actual values of n over all times and their predicted value computed from the above equation integrated over all spatial bins and time. The derivatives were not used in the fitting process due to the abrupt evolution of n over time, which required assumption of an appropriate functional form for n to compute a smoothly varying analytical derivative. The data used in these fits for

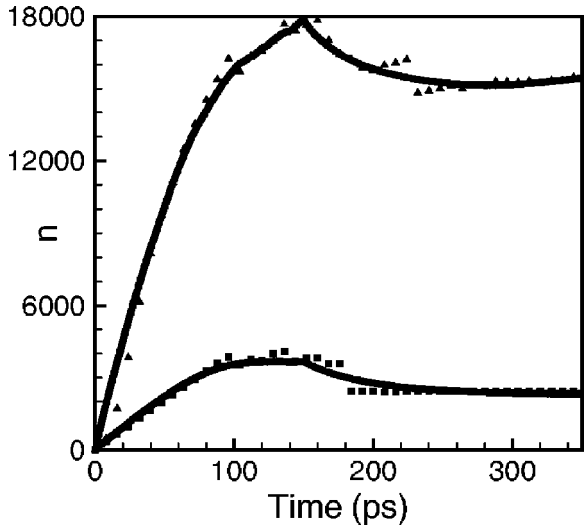

FIG. 8. The evolution of the total number of transformed beads, n, for Norrish type I (squares) and for Norrish type II (triangles) cases at 15 mJ/cm^2 fluence. The corresponding least squares fits are shown with solid lines.

the total number of transformed beads exclude the number of beads forming small gaseous molecules. This exclusion is required because even though the small gas molecules are generated via a photochemical process and are amenable to modeling using the first term in the above equation, their ejection is not a thermally activated process as already discussed. Also, an additional Arrhenius reaction term was used to account for a continued generation of MMA monomers by propagating radicals in the Norrish type II case.

The fits, shown in Fig. 8, provide a remarkably good qualitative description of the evolution of the number of transformed materials with the following parameter sets: $(2.2\times10^9\ s^{-1},\ 2.2\times10^{12}\ s^{-1},\ 1.6\ eV)$ for Norrish type I and $(1.1\times10^{10}\ s^{-1},\ 6.5\times10^{12}\ s^{-1},\ 1.7\ eV)$ for Norrish type II. No fit to the 20 mJ/cm^2 fluence data was performed as the abrupt transitions in n over time, caused by the breaking off of large polymer fragments, are not well captured by the above equation. This can be attributed to the small value of penetration depth and, consequently, to the higher energy density established on the top layers of the substrate. The ejection of small molecules, which itself evolves smoothly over time, can also contribute to the process of abrupt removal of large fragments of the transformed substrate. The lower values of k_φ in Norrish type I cases are due to the exclusion of small molecules which can form 50% or more of the total number of transformed beads as well as the higher degree of transformation achieved in Norrish type II cases (Fig. 7). Note that the above equations provide only a macroscopic description of the process as they disregard all the microscopic constituents in our MD model such as the absorption of photons, bond breaks, and competing reactions leading to the formation of a range of transformed products. The description is also incomplete and lacks predictive capability as it only models part of the transformed material and does not account for the small molecules. An inherent feature of these equations is the direct decomposition of polymers into products via laser absorption. This suggests that thermal ablation models can also work just as well by accounting for photochemical bond breaks and the formation of gaseous products in addition to the thermally activated bond breaks.[18,19]

C. Substrate temperature and plume composition

The temperatures observed in our simulations are much higher than those reported in experiments (500–1000 K).[12,13,25,35,57,58] The MD model used in our study lacks the electronic degrees of freedom and has fewer atomic degrees of freedom (both translational and rotational) mainly due to coarse graining of the polymer. These missing components result in a lower than realistic heat capacity, poorer conductivity, and instantaneous conversion of all photon energy to heat. The combined effect of these alterations in parameters is higher than expected temperatures which can, in principle, initiate rapid thermal decomposition of the polymer precluding photochemical bond breaks and other chemical reactions.[17,63] No such outcome is observed as a result of the high temperatures in our simulation time frame. The various chemical reactions used in our simulations are favored and rapid compared to thermally stimulated polymer bond breaking. The polymer unzipping reaction, primarily responsible for the thermal breakdown of PMMA into MMA monomers at high temperatures, is also slower compared to other reactions involving the formation of small gaseous molecules. Nevertheless, the process of thermal decomposition of polymer is likely to dominate over longer time scales, as witnessed in our simulations. Longer time simulations (up to 2 ns) suggest a maximum surface temperature dropping to a more acceptable value of about 1000 K in roughly 3–5 ns time range mainly via thermal conduction of heat deeper into the sample and evaporation at the top surface. This cooling time scale is comparable to the pulse width of lasers used in experimental studies.[17,63]

The response of the substrate to different photoexcitation pathways can be distinguished based on the efficiency of the utilization of the incident laser energy. This incident energy manifests itself as increased thermal (kinetic) energy and altered chemical composition, i.e., changes in interaction (potential) energy, of the substrate. The efficiency can be defined as the fraction of incident laser energy carried away by the plume, measured in terms of changes to its total (potential and kinetic) energy with respect to the original substrate. For the heating cases, this is negligible at 8 mJ/cm^2, rising up to 35%–48% by 15–20 mJ/cm^2, for both pulse widths. In contrast, for the Norrish type I case, we get 40% efficiency at 8 mJ/cm^2, increasing to 65%–72% at higher fluences. The Norrish type II efficiencies lie in between these two cases as it contains a mixture of photochemical and photothermal processes. It is apparent from these results that the photochemical processes, when compared to the photothermal processes, are more efficient at utilizing the incident laser energy in the ablation regime, resulting in more ejected materials. However, the higher efficiencies in photochemical cases do not imply a cooler substrate because the chemical reactions transform the materials, releasing excess energy as heat.

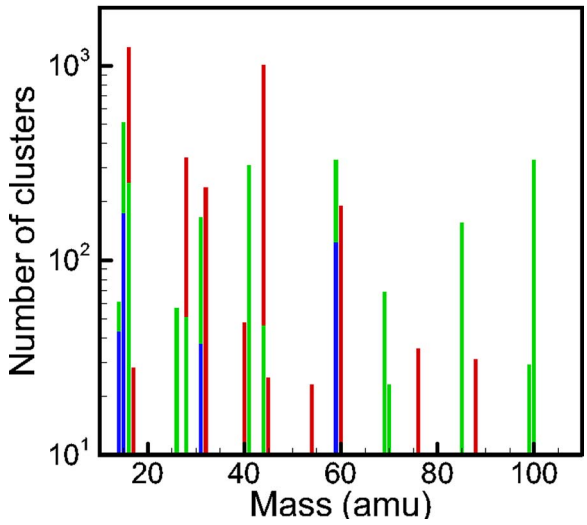

FIG. 9. (Color online) Chemical composition of the ablation plumes at fluence of 15 mJ/cm^2 and τ=150 ps for heating (blue), Norrish type I (red), and Norrish type II (green) reaction cases. Only clusters in the mass range of 10–100 amu are shown.

The efficiency of the generation of small molecules via thermally activated mechanisms in the heating case is very small, as demonstrated in Fig. 9, showing the chemical composition of the ablation plume, for 15 mJ/cm^2 fluence and τ=150 ps, evaluated at the end of the run. All the small molecules formed in the heating case are shown in Fig. 9, and more are expected to form via evaporation from substrate and gradual decomposition of plume over macroscopic time scales. The peaks in Fig. 9 are located at masses 14, 15, 31, and 59 corresponding to CH_2, CH_3, CH_3O, and CH_3COO fragments. Few (approximately ten) intact MMA fragments are seen in spite of a large number of C–CH_2 thermal bond breaks. For the Norrish type I reactions, CO_2 molecules (mass 44) form about 20%, and CH_4 (mass 16) another 10% of the total (number) yield at 15 mJ/cm^2. Carbon monoxide, methanol, and methyl formate (peaks at 28, 32, and 60) are only formed in smaller quantities at about 20% of the molecular yield of CO_2. This yield fraction stays constant as a fraction of the CO_2 yield. There is not any significant number of radicals ejected ($<1\%$) or leftover in the substrate at any fluence due to fast radical-radical recombination reactions. The product distribution is largely independent of the laser pulse widths. For the Norrish type II reactions, the bulk ($\sim 80\%-90\%$) of the yield above the ablation threshold is comprised of unzipped MMA units and polymer fragments (intact and thermally broken). Many other peaks, e.g., at masses of 15, 41, 59, and 85, corresponding to thermally broken polymer fragments are also seen in Fig. 9. The higher yield at τ=150 ps reported in Table I is entirely due to clusters smaller than one MMA unit, which are formed because more reactions and more thermal damage are possible for the longer pulse width with a longer ejection time scale. Small amounts of CH_4 molecules are formed at about 10%–15% of the total MMA equivalent yield in case of Norrish type II reactions.

The numbers seen in Fig. 9, for the heating case, will probably not be adequate to account for all the small molecules observed in the ablation plume experimentally. In contrast, the two Norrish reaction scenarios create a large number of smaller volatile molecules, up to ten times greater than in the heating case. This difference does not directly affect the yield in any significant manner as the thermal ablation yields are within a factor of 2 of the photochemical yields in the worst case (Table I), but it plays a key role in guiding the ablation process differently. These reaction products also drive the postablation dynamics in the plume, which is absent in the heating case. The characteristics of the ablation plume also changes with increasing fluence. Just above the ablation threshold, the plume consists mostly of thermally desorbed small molecules, but with increasing fluence, their proportion goes down and larger polymer fragments constitute the bulk of ablated materials. The larger clusters continue to disintegrate even after ejection, releasing small gaseous products and polymer fragments of which they are composed.

IV. CONCLUSIONS

We have developed a coarse-grained MD model to study the role of thermal, mechanical, and chemical reactions in the onset of ablation during UV laser irradiation of polymeric materials. The model utilizes well known and widely reported reaction chemistry of the PMMA polymer. The results discussed in this article elucidate possible mechanisms in action during laser ablation when the photon energy is absorbed in different ways, that is, pure heating, Norrish type I reactions, and Norrish type II reactions, in the PMMA substrate. Pressure and mechanical stresses are dominant for very short pulse widths in the stress confinement regime and can set off ablation by mechanical breakdown of the polymer matrix in the pure heating case. For the longer pulse width studied, however, the ejection process is predominantly thermally activated. Purely thermal models based on the thermally activated bond break process can work well in describing these events.

We find that the efficiency of a purely thermal mechanism in creating gaseous molecules is small, and the gaseous products observed during laser ablation experiments with PMMA using 157–308 nm wavelength lasers can only be accounted for by incorporating direct photochemical bond scission. The photoscission and subsequent reactions alter the substrate by causing rapid and nearly complete decomposition of the polymer matrix into smaller molecules. This alteration destroys the cohesive polymer matrix and removes the possibility of ablation via a mechanical failure for the Norrish reaction cases. The products of reactions, i.e., small molecules and polymer fragments, eject out rapidly from the substrate. This hollows out the substrate, further weakening it and causing larger clusters to eject. The mechanism of ejection of larger clusters in these cases is also thermal in nature. Modeling these photoablation channels requires a two step ablation model which incorporates the effect of the photolysis of polymer substrates and the creation of new species followed by a thermally activated removal step.

In this paper, we have presented many important aspects of the onset of ablation achieved via different energy depo-

sition pathways. The mechanistic differences observed among the three cases should serve us to better understand the contribution made by each in ablation experiments. In particular, the contribution of the small molecules, if detected, can provide a great insight to address the issues related to thermal versus photochemical ablation mechanisms. Our studies have shown a glimpse of the complexity involved in the interaction of lasers with polymeric materials and have highlighted the usefulness of treating the competing pathways separately. Further studies at longer wavelengths and larger penetration depths along with mixed photochemical-photothermal scenarios will provide a better mechanistic understanding of the ablation process under more realistic conditions.

ACKNOWLEDGMENTS

The authors would like to thank Dr. Leonid Zhigilei, Dr. R. Srinivasan, and Dr. Y. Yingling for helpful discussions. This work was supported by the National Science Foundation through the Information Technology Research Program, Grant No. 0426604, and the U.S. Air Force Office of Scientific Research through the Multi-University Research Initiative. The computer support was provided by the Academic Services and Emerging Technologies at Penn State University.

[1]F. Hillenkamp and M. Karas, Int. J. Mass. Spectrom. **200**, 71 (2000).
[2]R. E. Johnson, In *Large Ions: Their Vaporization, Detection and Structural Analysis*, edited by T. Baer, C. Y. Ng, and I. Powis (Wiley, New York, 1996), p. 49.
[3]N. H. Niemz, *Laser Tissue Interactions: Fundamentals and Applications*, 2nd ed. (Springer, Berlin, 2002), p. 303.
[4]P. E. Dyer, Appl. Phys. A: Mater. Sci. Process. **A77**, 167 (2003).
[5]D. Bäuerle, *Laser Processing and Chemistry* (Springer-Verlag, Berlin, 2000).
[6]C. Dorronsoro, D. Cano, J. Merayo-Lloves, and S. Marcos, Opt. Express **14**, 6142 (2006).
[7]R. Srinivasan, B. Braren, D. E. Seeger, and R. W. Dreyfus, Macromolecules **19**, 916 (1986).
[8]D. J. Krajnovich, J. Phys. Chem. A **101**, 2033 (1997).
[9]T. Efthimiopoulos, C. Kiagias, G. Heliotis, and E. Helidonis, Can. J. Phys. **78**, 509 (2000).
[10]T. H. Fedynyshyn, R. R. Kunz, R. F. Sinta, R. B. Goodman, and S. P. Doran, J. Vac. Sci. Technol. B **18**, 3332 (2000).
[11]M. Tsunekawa, S. Nishio, and H. Sato, J. Appl. Phys. **76**, 5598 (1994).
[12]R. Srinivasan and B. Braren, Chem. Rev. (Washington, D.C.) **89**, 1303 (1989).
[13]T. Lippert, R. L. Webb, S. C. Langford, and J. T. Dickinson, J. Appl. Phys. **85**, 1838 (1999).
[14]T. Lippert, Plasma Processes Polym. **2**, 525 (2005).
[15]S. Kuper, S. Modaressi, and M. Stuke, J. Phys. Chem. **94**, 7514 (1990).
[16]S. Kuper and M. Stuke, Appl. Phys. A: Solids Surf. **A49**, 211 (1989).
[17]T. Lippert and J. T. Dickinson, Chem. Rev. (Washington, D.C.) **103**, 453 (2003).
[18]N. Bityurin, B. S. Luk'yanchuk, M. H. Hong, and T. C. Chong, Chem. Rev. (Washington, D.C.) **103**, 519 (2003).
[19]H. Schmidt, J. Ihlemann, B. Wolff-Rottke, K. Luther, and J. Troe, J. Appl. Phys. **83**, 5458 (1998).
[20]N. Arnold, N. Bityurin, and D. Bauerle, Appl. Surf. Sci. **138–139**, 212 (1999).
[21]N. Bityurin and A. Malyshev, J. Appl. Phys. **92**, 605 (2002).
[22]H. H. G. Jellinek and R. Srinivasan, J. Phys. Chem. **88**, 3048 (1984).
[23]E. Sutcliffe and R. Srinivasan, J. Appl. Phys. **60**, 3315 (1986).
[24]B. J. Garrison and R. Srinivasan, Appl. Phys. Lett. **44**, 849 (1984).
[25]B. Danielzik, N. Fabricius, M. Rowekamp, and D. v. d. Linde, Appl. Phys. Lett. **48**, 212 (1986).
[26]R. C. Estler and N. S. Nogar, Appl. Phys. Lett. **49**, 1175 (1986).
[27]A. Gupta, R. Liang, F. D. Tsay, and J. Moacanin, Macromolecules **13**, 1696 (1980).
[28]P. E. Dyer and R. Srinivasan, J. Appl. Phys. **66**, 2608 (1989).
[29]N. Bityurin, Appl. Surf. Sci. **138–139**, 354 (1999).
[30]B. Luk'yanchuk, N. Bityurin, M. Himmelbauer, and N. Arnold, Nucl. Instrum. Methods Phys. Res. B **122**, 347 (1997).
[31]V. Srinivasan, M. A. Smrtic, and S. V. Babu, J. Appl. Phys. **59**, 3861 (1986).
[32]G. Paltauf and P. E. Dyer, Chem. Rev. (Washington, D.C.) **103**, 487 (2003).
[33]A. Vogel and V. Venugopalan, Chem. Rev. (Washington, D.C.) **103**, 2079 (2003).
[34]D. Perez and L. J. Lewis, Phys. Rev. B **67**, 184102 (2003).
[35]D. E. Hare, J. Franken, and D. D. Dlott, J. Appl. Phys. **77**, 5950 (1995).
[36]P. E. Dyer and J. Sidhu, J. Appl. Phys. **57**, 1420 (1985).
[37]D. R. Tyler, J. Macromol. Sci., Polym. Rev. **44**, 351 (2004).
[38]Y. G. Yingling, L. V. Zhigilei, and B. J. Garrison, J. Photochem. Photobiol., A **145**, 173 (2001).
[39]Y. G. Yingling and B. J. Garrison, J. Phys. Chem. B **108**, 1815 (2004).
[40]L. V. Zhigilei, E. Leveugle, B. J. Garrison, Y. G. Yingling, and M. I. Zeifman, Chem. Rev. (Washington, D.C.) **103**, 321 (2003).
[41]L. V. Zhigilei, P. B. S. Kodali, and B. J. Garrison, J. Phys. Chem. B **101**, 2028 (1997).
[42]L. V. Zhigilei and B. J. Garrison, J. Appl. Phys. **88**, 1281 (2000).
[43]Y. G. Yingling and B. J. Garrison, J. Phys. Chem. B **109**, 16482 (2005).
[44]W. K. Kim and L. M. Hayden, J. Chem. Phys. **111**, 5212 (1999).
[45]N. F. A. van der Vegt, W. J. Briels, M. Wessling, and H. Strathmann, J. Chem. Phys. **105**, 8849 (1996).
[46]S. B. Sane, T. Cagin, W. Knauss, and W. A. Goddard III, J. Comput.-Aided Mater. Des. **8**, 87 (2001).
[47]L. V. Zhigilei and B. J. Garrison, Mater. Res. Soc. Symp. Proc. **538**, 491 (1999).
[48]M. Prasad, P. F. Conforti, and B. J. Garrison, J. Chem. Phys. (submitted).
[49]P. F. Conforti and B. J. Garrison, Chem. Phys. Lett. **406**, 294 (2005).
[50]D. A. Good and J. S. Francisco, J. Phys. Chem. A **106**, 1733 (2002).
[51]M. Prasad, P. F. Conforti, and B. J. Garrison, Appl. Surf. Sci. **253**, 6382 (2007).
[52]G. B. Blanchet, P. Cotts, and C. R. Fincher, J. Appl. Phys. **88**, 2975 (2000).
[53]C. J. Kulik, Proc. SPIE **5339**, 35 (2004).
[54]D. Riedel and M. C. Castex, Appl. Phys. A: Mater. Sci. Process. **69**, 375 (1999).
[55]R. E. Gorga and R. E. Cohen, J. Polym. Sci., Part B: Polym. Phys. **42**, 2690 (2004).
[56]L. N. Andradi, B. L. Owenhaupt, A. Haufe, and G. P. Hellman, Angew. Makromol. Chem. **185–186**, 87 (1991).
[57]E. Rebollar, G. Bounos, M. Oujja, C. Domingo, S. Georgiou, and M. Castillejo, J. Phys. Chem. B **110**, 14215 (2006).
[58]B. Giannis, S. Alexandros, G. Savas, R. Esther, C. Marta, and B. Nikita, J. Appl. Phys. **100**, 114323 (2006).
[59]L. V. Zhigilei and B. J. Garrison, Appl. Phys. A: Mater. Sci. Process. **69**, S75 (1999).
[60]N. Bityurin, N. Arnold, B. Luk'yanchuk, and D. Bauerle, Appl. Surf. Sci. **127–129**, 164 (1998).
[61]P. F. Conforti, M. Prasad, and B. J. Garrison, Appl. Surf. Sci. **253**, 6386 (2007).
[62]L. I. Kalontarov and R. Marupov, Chem. Phys. Lett. **196**, 15 (1992).
[63]N. Bityurin, Annu. Rep. Prog. Chem., Sect. C: Phys. Chem. **101**, 216 (2005).